

# Role of Spin-Orbit Coupling on the Spin Triplet Pairing in $\text{Na}_x\text{CoO}_2 \cdot y\text{H}_2\text{O}$

## II: Multiple phase diagram under the Magnetic Field

Youichi YANASE\*, Masahito MOCHIZUKI and Masao OGATA

*Department of Physics, University of Tokyo, Tokyo 113-0033*

(Received Today 2005)

The possibility of multiple phase diagram in the novel superconductor  $\text{Na}_x\text{CoO}_2 \cdot y\text{H}_2\text{O}$  is analyzed on the basis of the multi-orbital Hubbard model including the atomic spin-orbit coupling. We have shown that the spin triplet pairing state is stable in this model. The  $p$ -wave ( $f$ -wave) state is stabilized when the Hund's rule coupling is large (small). In the precedent paper, we have determined the direction of  $d$ -vector at  $T = T_c$  and  $H = 0$  within the linearized Dyson-Gorkov equation. In this paper, the pairing state below  $T_c$  and under the magnetic field is determined within the weak coupling approximation including the paramagnetic effect. We find that the  $p+f$  coexistent state is stabilized at low temperatures in a part of parameter range. We point out that the phase diagram in the  $H$ - $T$  plane is quite different between the  $p$ -wave,  $f$ -wave and  $p+f$ -wave superconductivities. The characteristics of each phase are clarified by showing the magnetic susceptibility and specific heat. We discuss the comparison with experimental results and suggest some future experiments to detect the multiple phase transition.

KEYWORDS:  $\text{Na}_x\text{CoO}_2 \cdot y\text{H}_2\text{O}$ ; multi-orbital model; spin triplet superconductivity;  $d$ -vector; multiple phase diagram

### 1. Introduction

The spin triplet superconductivity is one of the most exciting topics in condensed matter physics. Vast studies have been devoted to the candidate materials such as  $\text{Sr}_2\text{RuO}_4$ ,<sup>1)</sup>  $(\text{TMTSF})_2\text{PF}_6$ ,<sup>2)</sup>  $\text{UPt}_3$ ,<sup>3)</sup>  $\text{UNi}_2\text{Al}_3$ ,<sup>4)</sup>  $\text{UGe}_2$ <sup>5)</sup> and  $\text{URhGe}$ .<sup>6)</sup> Recently, a novel superconductivity has been discovered in  $\text{Na}_x\text{CoO}_2 \cdot y\text{H}_2\text{O}$ <sup>7)</sup> and the possibility of spin triplet superconductivity has attracted huge interests.

The properties of superconducting state in  $\text{Na}_x\text{CoO}_2 \cdot y\text{H}_2\text{O}$  have been investigated by many experimental studies including the magnetization,<sup>8)</sup> NMR,<sup>9-13)</sup>  $\mu\text{SR}$ ,<sup>14-16)</sup> specific heat,<sup>17-19)</sup> resistivity,<sup>20)</sup> and impurity effect.<sup>21)</sup> Except for the impurity effect,<sup>21)</sup> most of them indicate a non- $s$ -wave pairing. The discovery of magnetic phase in the neighborhood of superconducting phase<sup>22,23)</sup> indicates a strong electron correlation which generally leads to an unconventional superconductivity.

As summarized in Ref. 24, there have been many theoretical studies.<sup>25-35)</sup> Although most of these studies have assumed single-orbital models, the justification of this assumption is not clear because the conduction band in  $\text{Na}_x\text{CoO}_2 \cdot y\text{H}_2\text{O}$  has orbital degeneracy, as pointed out by Koshibae *et al.*<sup>36)</sup> In order to examine the superconductivity in the multi-orbital system, we have constructed a three-orbital Hubbard model<sup>37)</sup> which appropriately reproduces the electronic structure obtained in the LDA calculations.<sup>38-40)</sup> From the results of perturbation theory<sup>41)</sup> and FLEX approximation,<sup>37)</sup> we have shown that the spin triplet superconductivity is stable in the wide parameter range. Then, the  $p$ -wave superconductivity and  $f$ -wave superconductivity are nearly degenerate because of the character of orbital in each Fermi surface.<sup>41)</sup> We have found an orbital dependent superconductivity like  $\text{Sr}_2\text{RuO}_4$ <sup>42)</sup> and derived the two-orbital Hubbard model reproducing the  $e'_g$ -doublet which

mainly leads to the superconductivity.

In the precedent paper,<sup>24)</sup> which we call "I" in the following, we have constructed a two-orbital Hubbard model including the spin-orbit coupling term and determined the  $d$ -vector at  $T = T_c$  with use of the linearized Dyson-Gorkov equation. In the present paper, we study the phase diagram in the temperature and the magnetic field plane ( $H$ - $T$  plane) and clarify the physical properties, such as magnetic susceptibility and specific heat, in each phase. This study is for the following two purposes. (1) One purpose is to provide clear physical quantities which can be compared in experiments. Many measurements including the NMR Knight shift are performed under the magnetic field. Since the  $d$ -vector may rotate under the magnetic field so as to gain the Zeeman coupling energy, it is highly desired to understand the  $d$ -vector under the magnetic field. (2) Another and more interesting purpose is to suggest a possibility of multiple phase transition in the superconducting state. The multiple phase diagram may appear in the  $H$ - $T$  plane owing to the rotation of  $d$ -vector. If the multiple phase transition is observed in experiments, that will be a strong evidence for the spin triplet pairing.

The effects of spin-orbit coupling were clarified in I. In the model without any spin-orbit coupling term, the  $d$ -vector rotates in the infinitesimal magnetic field. In general, the  $d$ -vector is determined by the competition between the magnetic field and the anisotropy arising from the spin-orbit coupling. For superconductors, it is reasonable to consider the atomic spin-orbit coupling, namely so-called  $L$ - $S$  coupling as a microscopic origin of the spin-orbit coupling for Cooper pairs. Therefore, the  $d$ -vector in spin triplet superconductors is a fundamental issue of multi-orbital systems.

The multiple phase transition in heavy fermion superconductors has attracted much interests for last two

decades.<sup>43–46)</sup> Then, the theoretical treatment has relied on the phenomenological theory and the role of  $L$ - $S$  coupling on the  $d$ -vector has been a longstanding problem. For instance, the pairing symmetry in  $\text{UPt}_3$  has been discussed for a long time and the anisotropy of  $d$ -vector is still under debate.<sup>43–45)</sup> We consider that the study on the  $d$ -electron systems will be a first step for this problem. The microscopic theory including the spin-orbit coupling can be applied to the  $d$ -electron systems like  $\text{Na}_x\text{CoO}_2 \cdot y\text{H}_2\text{O}$  and  $\text{Sr}_2\text{RuO}_4$  because these systems have a simple electronic structure in comparison with  $f$ -electron systems. Actually, we have performed a microscopic analysis on the  $d$ -vector in  $\text{Sr}_2\text{RuO}_4$ <sup>47,48)</sup> and obtained the consistent results with experiments.<sup>49,50)</sup> We have found that  $\text{Sr}_2\text{RuO}_4$  is a particular case in the sense that the anisotropy of  $d$ -vector is very small owing to the orbital dependent superconductivity. This result has been confirmed by the NMR measurement.<sup>50)</sup> In this paper, we show that  $\text{Na}_x\text{CoO}_2 \cdot y\text{H}_2\text{O}$  is a more general case where the spin-orbit coupling plays a more important role. We point out that the multiple phase transition will occur when the order parameter includes the  $p$ -wave component.

This paper is organized as follows. In §2, we briefly summarize the results of linearized Dyson-Gorkov equation for the two-orbital Hubbard model and derive an effective single-band model including the Zeeman coupling term. In §3, we determine the phase diagram in  $H$ - $T$  plane within the mean field theory. We obtain three pairing states at zero magnetic field, namely the  $p$ -wave,  $f$ -wave and  $p + f$ -wave states. The  $d$ -vector under the magnetic field are investigated for these states in §3.1, §3.2 and §3.3, respectively. Our interests are focused on the magnetic field parallel to the two-dimensional plane because a wide variety of phase diagram is expected in this direction and also because the Knight shift has been measured under the parallel magnetic field in most cases.<sup>9,10,13,14,51,52)</sup> The nature of multiple phase transition is analyzed with attention to the thermal and magnetic properties. In §4, the role of vortex state and that of  $a_{1g}$ -orbital which are ignored in §3 will be discussed. We show that an extra phase transition may be induced by these effects. Some discussions are given in the last section §5.

## 2. Formulation

### 2.1 Pairing state at $T = T_c$ and $H = 0$

As in I, we adopt a two-orbital Hubbard model reproducing the  $e'_g$ -doublet. From the analysis of three orbital Hubbard model without including the spin-orbit coupling, we have found that the superconductivity is mainly induced by the  $e'_g$ -orbitals.<sup>37,41)</sup> Indeed, the two-orbital Hubbard model without including the  $a_{1g}$ -orbital appropriately reproduces the results of three-orbital Hubbard model.<sup>41)</sup> We choose the parameters of two-orbital Hubbard model as in I<sup>24)</sup> unless we specify.

The pairing symmetry in the two-orbital and three-orbital Hubbard models are basically determined by the two parameters, namely  $n_e$  and  $J_H$ . Here,  $n_e$  is the holes in the  $e_g$ -Fermi surface and  $J_H$  is the Hund's rule coupling. We have found that the  $f$ -wave superconductivity

is favored when  $n_e$  is large and *vice versa*.<sup>24,41)</sup> This is because the amplitude of order parameter in the  $p$ -wave symmetry have to be small around the K-point owing to the periodicity of Brillouin zone. As increasing  $n_e$ , the  $e_g$ -Fermi surface approaches to the K-point and the  $p$ -wave superconductivity becomes unfavorable. As for  $J_H$ , the  $p$ -wave ( $f$ -wave) superconductivity is stabilized when  $J_H$  is large (small).

The  $d$ -vector is determined by the spin-orbit coupling term which plays an essential role for the issues in this paper. The coupling constant  $2\lambda$  of spin-orbit coupling term has been estimated as 57meV from NMR measurements.<sup>53)</sup> This value corresponds to  $\lambda = 0.17$  in our unit if we choose the band width  $W \sim 9 = 1.5\text{eV}$  according to the LDA calculations. Although this estimation has some ambiguities, the spin-orbit coupling in this order is much smaller than the band width. This is in contrast with the RVB theory discussed by Khaliullin *et al.*<sup>35)</sup> who have considered the opposite limit  $\lambda = \infty$ .

If the spin-orbit coupling is neglected, there remains a  $3 \times 2 = 6$ -fold degeneracy in the  $p$ -wave state, while the degeneracy in the  $f$ -wave state is 3-fold. Due to the spin-orbit coupling, the degeneracy is lifted and the pairing states are classified into  $P_{xy+}$ ,  $P_{xy-}$  and  $P_z$  for the  $p$ -wave symmetry while  $F_{xy}$  and  $F_z$  for the  $f$ -wave symmetry. The  $d$ -vector in these states has been summarized in Table II of I.<sup>24)</sup> We have determined the pairing state at  $T = T_c$  and  $H = 0$  with use of the linearized Dyson-Gorkov equation whose derivation for the  $SU(2)$  asymmetric system has been given in I and Ref. 47. For the two-orbital Hubbard model, we have obtained the two independent equations as,

$$\lambda_e^{\uparrow\uparrow} \Delta_{\uparrow\uparrow}(k) = - \sum_{k'} V_{\uparrow\uparrow}(k, k') |G_2(k')|^2 \Delta_{\uparrow\uparrow}(k'), \quad (1)$$

$$\lambda_e^{\uparrow\downarrow} \Delta_{\uparrow\downarrow}(k) = - \sum_{k'} V_{\uparrow\downarrow}(k, k') |G_2(k')|^2 \Delta_{\uparrow\downarrow}(k'). \quad (2)$$

Here,  $\Delta_{\uparrow\uparrow}$  and  $\Delta_{\uparrow\downarrow}$  are the order parameters for the equal spin pairing state and opposite spin pairing state, respectively. For the effective interactions,  $V_{\uparrow\uparrow}(k, k')$  and  $V_{\uparrow\downarrow}(k, k')$ , we applied the second order perturbation theory (SOP) with respect to the Coulomb interactions, *i.e.*  $U$ ,  $U'$ ,  $J_H$  and  $J$ . Note that we have confirmed that the SOP is consistent with the renormalized third order perturbation theory as well as the FLEX approximation which include higher order corrections.<sup>37,41)</sup> The Green function  $G_2(k)$  is defined as  $G_2(k) = \frac{1}{i\omega_n - E_2(\mathbf{k})}$  where  $E_2(\mathbf{k})$  is the upper band composing the Fermi surface. Note that  $E_2(\mathbf{k})$  is slightly affected by the spin-orbit coupling.

By solving eqs. (1) and (2), we have found that the spin-orbit coupling stabilizes the  $P_{xy+}$ -state when the pairing symmetry is  $p$ -wave. Then, the pairing state is described by the  $d$ -vector as,  $\hat{d} = p_x \hat{x} + p_y \hat{y}$  or  $\hat{d} = p_y \hat{x} - p_x \hat{y}$ . There is no violation of time-reversal-symmetry in this state which is consistent with the  $\mu\text{SR}$  measurement.<sup>14)</sup> In the case of  $f$ -wave symmetry,  $F_{xy}$ -state ( $\hat{d} = f_1 \hat{x} - \alpha f_2 \hat{y}$  or  $\hat{d} = \alpha f_2 \hat{x} + f_1 \hat{y}$ ) and  $F_z$ -state ( $\hat{d} = f_1 \hat{z}$ ) can be stabilized depending on  $n_e$  and  $J_H$ .

As shown in I, the anisotropy of  $d$ -vector defined as

$|\lambda_e^{\uparrow\uparrow} - \lambda_e^{\downarrow\downarrow}|/\lambda_e^{\uparrow\uparrow}$  is much larger in the  $p$ -wave state than in the  $f$ -wave state. This is because the first order term in spin-orbit coupling vanishes in the latter case. This means that the  $d$ -vector in the  $f$ -wave superconductivity is rotated by a small magnetic field parallel to the  $d$ -vector. Thus, the role of spin-orbit coupling is quite different between the  $p$ -wave and  $f$ -wave superconductivities. This leads to the qualitatively different phase diagram under the magnetic field as shown in §3.1-3.

## 2.2 Weak coupling approximation

In order to determine the pairing state below  $T_c$  and under the magnetic field, we introduce an effective single-band model which reproduces the results of linearized Dyson-Gorkov equation at  $H = 0$ .

$$\begin{aligned}
H_1 = & \sum_{k,s} E_2(\mathbf{k}) c_{k,s}^\dagger c_{k,s} \\
& - \frac{1}{2} g_1 \sum_{k,k',s} \phi_{1x}(\mathbf{k}) \phi_{1x}(\mathbf{k}') c_{k,s}^\dagger c_{-k',s}^\dagger c_{-k',s} c_{k',s} \\
& - \frac{1}{2} g_2 \sum_{k,k',s} \phi_{1y}(\mathbf{k}) \phi_{1y}(\mathbf{k}') c_{k,s}^\dagger c_{-k',s}^\dagger c_{-k',s} c_{k',s} \\
& - \frac{1}{2} g_3 \sum_{k,k',s} [i s \phi_{1x}(\mathbf{k}) \phi_{1y}(\mathbf{k}') c_{k,s}^\dagger c_{-k',s}^\dagger c_{-k',s} c_{k',s} \\
& \quad - i s \phi_{1y}(\mathbf{k}) \phi_{1x}(\mathbf{k}') c_{k,s}^\dagger c_{-k',s}^\dagger c_{-k',s} c_{k',s}] \\
& - \frac{1}{2} g_4 \sum_{k,k',s} \phi_{2x}(\mathbf{k}) \phi_{2x}(\mathbf{k}') c_{k,s}^\dagger c_{-k,-s}^\dagger c_{-k,-s} c_{k',s} \\
& - \frac{1}{2} g_5 \sum_{k,k',s} \phi_{2y}(\mathbf{k}) \phi_{2y}(\mathbf{k}') c_{k,s}^\dagger c_{-k,-s}^\dagger c_{-k,-s} c_{k',s} \\
& - \mathbf{M} \mathbf{H}, \tag{3}
\end{aligned}$$

where  $c_{k,s}^\dagger$  is the creation operator for the  $E_2(\mathbf{k})$ -band electron with pseudospin  $s$ . The coupling constants  $g_i$  are determined so as to reproduce the result of linearized Dyson-Gorkov equation, namely eqs. (1) and (2). Therefore, these parameters are determined by the microscopic parameters of Hubbard model such as  $n_e$  and  $J_H$ . Here,  $\phi_{1x}(\mathbf{k})$  and  $\phi_{1y}(\mathbf{k})$  are the orbital part of Cooper pair wave function for the  $d$ -vector along the plane which are determined by the linearized Dyson-Gorkov equation in eq. (1). For instance, we obtain  $\Delta_{\uparrow\uparrow}(\mathbf{k}, i\pi T) = -\phi_{1x}(\mathbf{k}) + i\phi_{1y}(\mathbf{k})$  when the  $P_{xy+}$ -state is stabilized at  $T = T_c$ . Similarly,  $\phi_{2x}(\mathbf{k})$  and  $\phi_{2y}(\mathbf{k})$  are the wave function for the  $d$ -vector along  $z$ -axis determined by eq. (2). In case of the  $p$ -wave superconductivity,  $\phi_{ix}(\mathbf{k})$  and  $\phi_{iy}(\mathbf{k})$  ( $i = 1, 2$ ) denote the wave functions in the  $p_x$ - and  $p_y$ -wave symmetry, respectively. In case of the  $f$ -wave superconductivity, these are wave functions in the  $f_2$ - and  $f_1$ -wave symmetry, respectively. We have neglected the frequency dependence of  $\phi_{i\alpha}(\mathbf{k})$  for simplicity and use the value at  $\omega_n = i\pi T$ , *i.e.* the smallest Matsubara frequency.

As a role of the magnetic field, we take into account the Zeeman coupling term, namely the last term in eq. (3). This term plays an essential role for the rotation of  $d$ -vector. We obtain the magnetic moment from the

two-orbital Hubbard model as  $M_\alpha = (L_\alpha + 2S_\alpha)\mu_B = \sum_{\mathbf{k}} g_\alpha(\mathbf{k}) \tilde{S}_\alpha(\mathbf{k}) \mu_B$  where  $\tilde{S}_\alpha$  is the operator of pseudospin for the  $E_2(\mathbf{k})$ -band electron. Here, the momentum dependent  $g$ -factor is obtained as  $g_\alpha(\mathbf{k}) = 2 < \mathbf{k}, \tilde{S}_\alpha = \frac{1}{2} [L_\alpha + 2S_\alpha | \mathbf{k}, \tilde{S}_\alpha = \frac{1}{2} \rangle >$  where  $|\mathbf{k}, \tilde{S}_\alpha = \frac{1}{2} \rangle$  is the wave function of  $E_2(\mathbf{k})$ -band with  $\tilde{S}_\alpha = \frac{1}{2}$ . Note that  $\alpha = x, y$  and  $z$  is the symmetry axis of crystal and  $g_x(\mathbf{k}) = g_y(\mathbf{k}) \neq g_z(\mathbf{k})$ . In the following, we consider the magnetic field along  $x$ -axis unless we mention.

In the following calculation, we simply ignore the orbital effect which induces the vortex state. We discuss the orbital effect in §4.1 and show that the phase diagram in the high field region  $H \sim H_{c2}$  can be affected when the orbital part of order parameter has multi-component as in the  $p$ -wave superconductivity.

Because we have assumed separable pairing interactions, the following two effects are ignored in eq. (3). First, although the momentum dependence of wave functions  $\phi_{i\alpha}(\mathbf{k})$  ( $i = 1, 2$  and  $\alpha = x, y$ ) depends on the temperature and magnetic field in general,<sup>46)</sup> we have ignored this deformation of  $\phi_{i\alpha}(\mathbf{k})$ . Second, the feedback effect, namely the effect of superconductivity on the effective interaction  $V_{ss'}(k, k')$  is neglected. Although a part of the feedback effect can be represented by the temperature dependence of attractive interaction, we have introduced temperature independent coupling constants  $g_i$  in eq. (3). These simplifications are justified in the weak coupling region  $T_c/W \ll 1$  which is reasonable in  $\text{Na}_x\text{CoO}_2 \cdot y\text{H}_2\text{O}$ . Qualitatively the same assumptions have been adopted in the analysis of  $\text{Sr}_2\text{RuO}_4$ .<sup>54)</sup>

In principle, these effects can be taken into account in the non-linear Dyson-Gorkov equation for the two-orbital Hubbard model including the Zeeman coupling term. However, the small value of transition temperature  $T_c \sim 5\text{K}$  makes the numerical calculation very difficult. Note that we have to calculate at  $T \sim 0.5\text{K}$  in order to determine the pairing state at  $T = 0.1T_c$ . The extraordinary large size simulation is needed to discuss such a small energy scale. If a larger value of  $T_c$  than 5K is assumed to enable the numerical calculation, we will overestimate contributions ignored in the weak coupling theory. For instance, the renormalization of effective interaction due to the superconducting order parameter is overestimated. As for the effect of magnetic field, the contributions scaled by  $\mu_B H/W$  are also overestimated, although only the contributions scaled by  $\mu_B H/T_c$  are taken into account in the weak coupling limit  $T_c/W \rightarrow 0$ . It is reasonable to consider that  $\text{Na}_x\text{CoO}_2 \cdot y\text{H}_2\text{O}$  is in the weak coupling region  $T_c/W \ll 0$  since  $T_c \sim 5\text{K}$ . Therefore, we take the weak coupling limit from the beginning and solve the weak coupling model in eq. (3) within the mean field theory.

In the following, we solve the mean field equation for  $H_1$  and find out the local minimum and saddle point of the free energy by performing the stability analysis. As a result, we search the minimum of the free energy and determine the phase transition. It should be noticed that the symmetry of Hamiltonian is reduced by the parallel magnetic field which we focus on. Then, we can only rely on the  $U(1)$  gauge symmetry and there are  $6 \times 2 - 1 =$

11 independent order parameters including the relative phase.

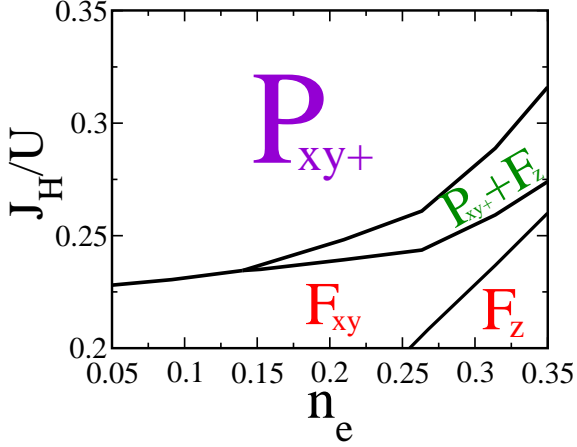


Fig. 1. Pairing state at  $H = 0$  and  $T = 0.1T_c^0$ . Here,  $T_c^0$  is the transition temperature at which the superconducting instability occurs, and we choose the parameter  $U$  so that  $T_c^0 = 6\text{K}$ . The notations of  $P_{xy+}$ ,  $F_{xy}$  and  $F_z$  have been given in Table II in I.<sup>24</sup> In the  $P_{xy+} + F_z$ -state, order parameters in the  $P_{xy+}$ - and  $F_z$ -states coexist.

Before showing the result under the magnetic field, we show the phase diagram at  $H = 0$  and below  $T_c$  in Fig. 1. We see the four states including the  $P_{xy+} + F_z$ -state. In this state, the  $p$ -wave order parameter with  $d$ -vector parallel to the plane coexists with the  $f$ -wave order parameter which has the  $d$ -vector along  $z$ -axis. This coexistent state is stabilized around the phase boundary between the  $p$ -wave and  $f$ -wave states so as to gain the condensation energy by making the superconducting gap more isotropic. In this paper, we denote this pairing state as  $p + f$ -wave state, for simplicity. In a small part of the parameter range, another pairing state such as  $P_z + F_{xy}$ -state may be stable. However, we ignore this possibility since the parameter region will be very small.

As will be shown in the following sections, the pairing state under the magnetic field is determined by three effects. (I) The spin-orbit coupling term which favors the pairing state shown in Fig. 1. (II) The magnetic field which is unfavorable for the  $d$ -vector parallel to the field. (III) The momentum dependence of the superconducting gap, *i.e.* the more isotropic superconducting gap is, the more condensation energy is gained below  $T_c$ . The multiple phase diagram appears in the  $H$ - $T$  plane as a result of these competing effects.

### 3. Phase Diagram under the Magnetic Field

In the following, we discuss the  $H$ - $T$  phase diagram in each case, *i.e.* the  $p$ -wave,  $f$ -wave and  $p + f$ -wave states. Hereafter, we choose the parameter  $U$  so that  $T_c^0 = 6\text{K}$  consistent with experimental value, where  $T_c^0$  is the transition temperature of superconductivity at  $H = 0$ . Note that  $T_c^0$  is the maximum value of transition temperatures for  $P_{xy+}$ -,  $F_{xy}$ - and  $F_z$ -states because the other state is not stabilized at  $T = T_c^0$  and  $H = 0$  in our calculation.<sup>24</sup>

#### 3.1 $P$ -wave state

First, we discuss the  $p$ -wave superconductivity which is realized in the large  $J_H$  region. We fix the parameters of two-orbital Hubbard model as  $J_H/U = 7/24$  and  $n_e = 0.21$  where we obtain  $T_c^0 = 6\text{K}$  by choosing  $U = 6.47$ . In the linearized Dyson-Gorkov equation for the equal spin pairing, (eq. (1)), we obtain the wave functions  $\phi_{1x}(\mathbf{k})$  and  $\phi_{1y}(\mathbf{k})$  as  $\Delta_{\uparrow\uparrow}(\mathbf{k}, i\pi T) = -\phi_{1x}(\mathbf{k}) + i\phi_{1y}(\mathbf{k})$  where  $\Delta_{\uparrow\uparrow}(\mathbf{k})$  is the eigenfunction corresponding to the maximum eigenvalue  $\lambda_e^{\uparrow\uparrow}$ . In eq. (2), we obtain  $\phi_{2x}(\mathbf{k})$  and  $\phi_{2y}(\mathbf{k})$  from doubly degenerate eigenfunctions as  $\Delta_{\uparrow\downarrow}(\mathbf{k}, i\pi T) = \phi_{2x}(\mathbf{k})$  and  $\Delta_{\uparrow\downarrow}(\mathbf{k}, i\pi T) = \phi_{2y}(\mathbf{k})$ . The difference between  $\phi_{1x}(\mathbf{k})$  and  $\phi_{2x}(\mathbf{k})$  and that between  $\phi_{1y}(\mathbf{k})$  and  $\phi_{2y}(\mathbf{k})$  are slight because  $\lambda \ll W$ . Because the amplitude of wave functions  $\phi_{i\alpha}(\mathbf{k})$  is not determined by the linearized Dyson-Gorkov equation, we impose the normalization condition for  $\phi_{i\alpha}(\mathbf{k})$  as,

$$K = \sum_{\mathbf{k}} \frac{|\phi_{i\alpha}(\mathbf{k})|^2}{2E_2(\mathbf{k})} \tanh \frac{E_2(\mathbf{k})}{2T_c^0} \quad (i = 1, 2 \text{ and } \alpha = x, y), \quad (4)$$

where  $K$  is an arbitrary value. Although the coupling constant  $g_i$  depends on the value of  $K$ , the physical quantities are obviously invariant for the choice of  $K$ .

According to the symmetry of triangular lattice, we obtain  $g_1 = g_2$  and  $g_4 = g_5$ . Then, we have three independent parameters, namely  $g_1$ ,  $g_3$  and  $g_5$ . At  $\lambda = 0$ , we obtain  $g_1 = g_5$  and  $g_3 = 0$ . Thus, the role of spin-orbit coupling is represented by the two parameters,  $g_1 - g_5$  and  $g_3$ .

The parameters  $g_1 + g_3$  and  $g_5$  are determined so as to reproduce the transition temperatures obtained in the linearized Dyson-Gorkov equation. From eq. (3), we obtain the gap equations at  $H = 0$  for the  $P_{xy+}$ - and  $P_z$ -states as,

$$1 = (g_1 + g_3) \sum_{\mathbf{k}} \frac{|\phi_{1x}(\mathbf{k})|^2}{2E_2(\mathbf{k})} \tanh \frac{E_2(\mathbf{k})}{2T_c^{(xy+)}}, \quad (5)$$

$$1 = g_5 \sum_{\mathbf{k}} \frac{|\phi_{2y}(\mathbf{k})|^2}{2E_2(\mathbf{k})} \tanh \frac{E_2(\mathbf{k})}{2T_c^{(z)}}. \quad (6)$$

Here,  $T_c^{(xy+)}$  is the transition temperature for the  $P_{xy+}$ -state, which is determined by the criterion  $\lambda_e^{\uparrow\uparrow} = 1$  at  $T = T_c^{(xy+)}$ , while  $T_c^{(z)}$  is the transition temperature for the  $P_z$ -state and determined by the criterion  $\lambda_e^{\uparrow\downarrow} = 1$  at  $T = T_c^{(z)}$ . Since  $T_c^{(xy+)} > T_c^{(z)}$  at  $H = 0$  as shown in Fig. 1, we obtain  $T_c^{(xy+)} = T_c^0 = 6\text{K}$ . We have obtained  $T_c^{(z)} = 0.865T_c^0$  for  $\lambda = 0.17$  by solving eq. (2). Thus,  $g_1 + g_3$  and  $g_5$  are determined by the microscopic parameters, such as  $U$ ,  $J_H$ ,  $n_e$  and  $\lambda$ , through  $T_c^{(xy+)}$  and  $T_c^{(z)}$ , respectively.

In principle, the parameter  $g_1 - g_3$  can be determined by the transition temperature for the  $P_{xy-}$ -state,  $T_c^{(xy-)}$  as,

$$1 = (g_1 - g_3) \sum_{\mathbf{k}} \frac{|\phi_{1x}(\mathbf{k})|^2}{2E_2(\mathbf{k})} \tanh \frac{E_2(\mathbf{k})}{2T_c^{(xy-)}}. \quad (7)$$

However, it is difficult to obtain the precise value of

$T_c^{(xy-)}$  from eq. (1) since  $T_c^{(xy-)} < T_c^{(xy+)}$ . Therefore, there remains an arbitrary parameter among  $g_1$  and  $g_3$ . This difficulty can be resolved by the microscopic analysis on the effective interactions  $V_{\uparrow\uparrow}(k, k')$  and  $V_{\uparrow\downarrow}(k, k')$ . As a result of the perturbation expansion in  $\lambda$ , we have found that  $|g_1 - g_5|$  is much smaller than  $|g_3|$ .<sup>24)</sup> The former is the second order term in  $\lambda$ , namely  $g_1 - g_5 = O(\lambda^2)$ , while the latter is the first order term, namely  $g_3 = O(\lambda)$ . Therefore, we assume  $g_1 - g_5 = 0$  for a while and we will show the role of finite value of  $g_1 - g_5$  later.

four phases A, B, C and D whose notations are given in Table I. The coefficients  $\alpha$  and  $\beta$  vary according to the magnetic field and temperature. We have not shown the small components in the order of  $O(T_c^0/W)$  which are induced by the magnetic field and particle-hole asymmetry. Strictly speaking, A-, B-, and D-phase are the non-unitary state owing to these small components. Recently, it has been pointed out that the non-unitarity induced by the paramagnetic effect plays an important role for  $\text{Sr}_2\text{RuO}_4$ .<sup>55)</sup> However, this effect is negligible in what follows since the spin-orbit coupling is much more significant for  $\text{Na}_x\text{CoO}_2 \cdot y\text{H}_2\text{O}$  than  $\text{Sr}_2\text{RuO}_4$ .<sup>24, 47)</sup>

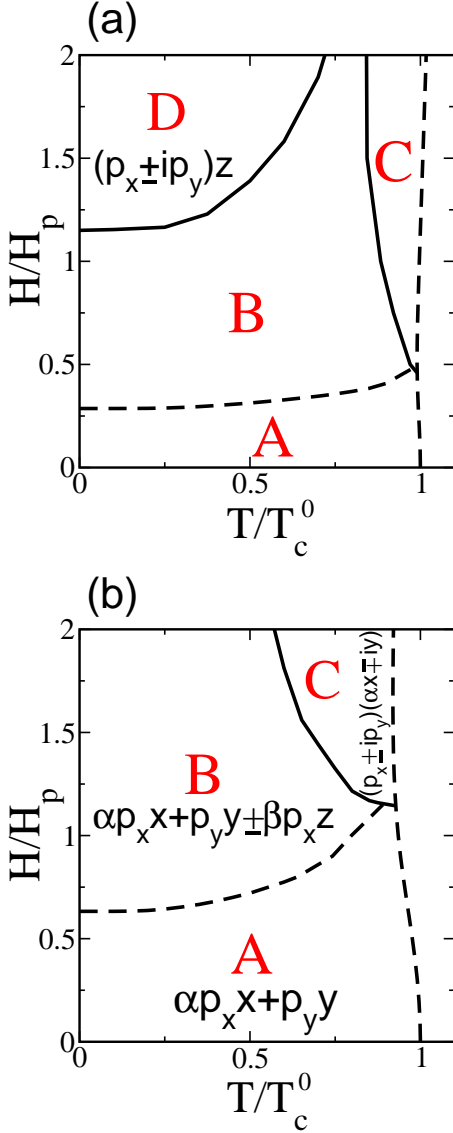


Fig. 2. The phase diagram in the  $p$ -wave superconducting state under the magnetic field along  $x$ -axis. We choose  $\lambda = 0.05$  in (a) and  $\lambda = 0.17$  in (b). The notations of A, B, C and D phases are given in Table I. The solid (dashed) line shows the first (second) order phase transition.

Figure 2 shows the phase diagram in  $H$ - $T$  plane for two values of  $\lambda$ . It should be noted that the effect of magnetic field is scaled by the typical value  $H_p$  which is defined as  $\mu_B H_p = k_B T_c^0$ . When we assume  $T_c^0 = 6\text{K}$ , we obtain  $H_p \sim 9\text{T}$ . Note that  $H_p$  is a slightly smaller value than the Pauli paramagnetic limit. We see in Fig. 2 the

A	$\alpha p_x \hat{x} + p_y \hat{y}$
B	$\alpha p_x \hat{x} + p_y \hat{y} \pm \beta p_x \hat{z}$
C	$(p_x \pm i p_y)(\alpha \hat{x} \mp i \hat{y})$
D	$(p_x \pm i p_y) \hat{z}$
E	$\alpha p_x \hat{x} + p_y \hat{y} \pm \beta f_1 \hat{z}$
F	$f_1 \hat{z}$

Table I. The pairing states under the magnetic field. The first column shows the notation in this paper. The second column shows the  $d$ -vector. Note that  $0 \leq \alpha, \beta \leq 1$ ,  $\frac{\partial \alpha}{\partial H} < 0$  and  $\frac{\partial \beta}{\partial H} > 0$ .

The A-phase is connected to the  $P_{xy+}$ -state at  $H = 0$  in an adiabatic way. This phase is favored by the spin-orbit coupling and stabilized at low magnetic fields. The  $\hat{x}$ -component of  $d$ -vector is reduced in the magnetic field so as to gain the Zeeman coupling energy, and therefore  $\frac{\partial \alpha}{\partial H} < 0$ . Note that the A-phase has a 2-fold degeneracy at  $H = 0$  or at  $T = T_c(H)$  where  $\hat{d} = \alpha p_x \hat{x} + p_y \hat{y}$  is degenerate with  $\hat{d} = \alpha p_y \hat{x} - p_x \hat{y}$ . This degeneracy is lifted for  $H \neq 0$  and  $T < T_c$ , and the former is stabilized because the order parameter in the  $p_y$ -wave symmetry  $\phi_{1y}(\mathbf{k})$  is more isotropic than that in the  $p_x$ -wave symmetry  $\phi_{1x}(\mathbf{k})$ . This lifting of degeneracy is very small and these two states are nearly degenerate. Therefore, it is expected that the orbital effect plays a more important role for the lifting of degeneracy. As will be discussed in §4.1, the degeneracy between  $\hat{d} = \alpha p_x \hat{x} + p_y \hat{y}$  and  $\hat{d} = \alpha p_y \hat{x} - p_x \hat{y}$  is lifted by the orbital effect, and the former is stabilized furthermore. According to the analysis on the Ginzburg-Landau free energy,<sup>42, 46, 56)</sup> the orbital effect on the lifting of this degeneracy is in the second order of order parameter, while the paramagnetic effect is beyond the fourth order.

The B-phase is stabilized at high magnetic fields. The reflection symmetry with respect to the  $xy$ -plane is violated in the B-phase. In comparison to the A-phase, the Zeeman coupling energy is gained in the B-phase because the  $x$ -component of  $d$ -vector is reduced, although the spin-orbit coupling term disfavors the B-phase. The A-B phase transition is described by the rotation of  $d$ -vector having the  $p_x$ -orbital component, which is shown in Fig. 3 schematically. It should be stressed that the  $\hat{x}$ -component of  $d$ -vector does not vanish even in the B phase owing to the  $g_3$ -term in eq. (3). Because the amplitude of  $p_x$ -wave order parameter increases as increasing the magnetic field across the A-B phase transition, the superconducting gap becomes more isotropic in the

B-phase. In comparison to the C-phase, the B-phase is stabilized at low temperatures since the superconducting gap is more isotropic in the spin space rather than the non-unitary C-phase. At high fields, the B'-phase where  $\hat{d} = \alpha p_y \hat{x} - p_x \hat{y} \pm \beta p_y \hat{z}$  is nearly degenerate with the B-phase and can be stabilized. However, we have ignored this possibility since the B'-phase is disfavored by the orbital effect which is discussed in §4.1.

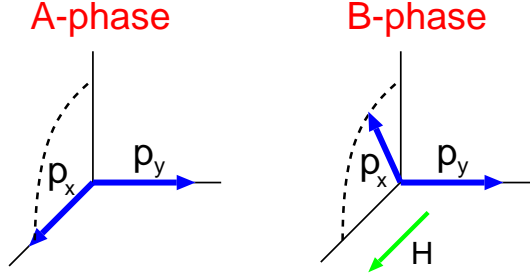


Fig. 3. The schematic figure for the A-B transition. The  $d$ -vector with  $p_x$ -wave symmetry rotates towards  $z$ -axis.

The C-phase is a non-unitary state, *i.e.*  $\hat{d} \times \hat{d}^* \neq 0$  where the time-reversal symmetry is broken. The C-phase can be stabilized just below  $T = T_c(H)$  because the  $d$ -vector is described by a linear combination of two-fold degenerate state at  $T = T_c(H)$  as  $\hat{d} = (\alpha p_x \hat{x} + p_y \hat{y}) \pm i(\alpha p_y \hat{x} - p_x \hat{y})$ . In general, a linear combination of the degenerate states is stabilized just below  $T_c(H)$  so as to make the superconducting gap most isotropic. The superconducting gap is more isotropic in the spin space in the unitary A-phase, while that is more isotropic in the momentum space in the C-phase owing to the factor  $p_x \pm ip_y$ . As increasing the magnetic field and therefore decreasing  $\alpha$ , the superconducting gap in the A-phase becomes anisotropic while that in the C-phase becomes isotropic. Therefore, the C-phase is stabilized at high fields. As decreasing the temperature, the B-phase is stable in comparison to the C-phase owing to the non-unitarity in the C-phase. Thus, the C-phase is stabilized at high magnetic fields and around  $T = T_c(H)$ .

The D-phase is the chiral superconducting state where the time-reversal-symmetry is broken. It has been expected that this phase is stabilized in  $\text{Sr}_2\text{RuO}_4$  at  $H = 0$ .<sup>1)</sup> However, the D-phase is not stabilized in  $\text{Na}_x\text{CoO}_2 \cdot y\text{H}_2\text{O}$  unless we assume a very small spin-orbit coupling as  $\lambda = 0.05$  in Fig. 2(a).

In the following part, we clarify the physical properties of each phase in order to compare with experimental results and to suggest future experiments. We first show the temperature dependence of magnetic susceptibility  $\chi = M/H$  in Fig. 4. It is clearly shown that the magnetic susceptibility is smaller than the normal state value in both A-phase and B-phase owing to the  $x$ -component of  $d$ -vector. The decrease of magnetic susceptibility is reduced by increasing the magnetic field since the  $x$ -component of  $d$ -vector decreases so as to gain the Zeeman coupling energy. These behaviors are qualitatively consistent with the recent NMR measurements in

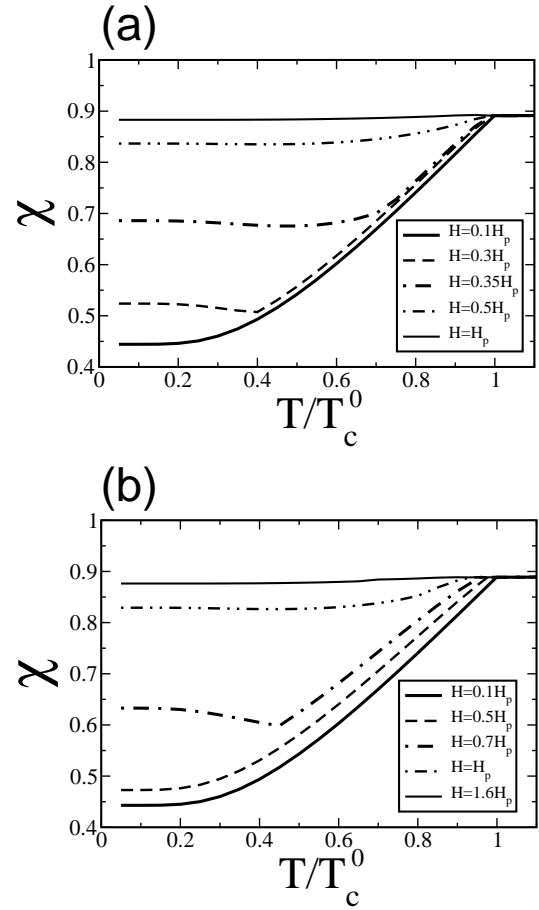


Fig. 4. The temperature dependence of magnetic susceptibility,  $\chi = M/H$ . (a)  $\lambda = 0.05$  and  $H = 0.1H_p, 0.3H_p, 0.35H_p, 0.5H_p$  and  $H_p$ . (b)  $\lambda = 0.17$  and  $H = 0.1H_p, 0.5H_p, 0.7H_p, H_p$  and  $1.6H_p$ .

the O-site.<sup>13)</sup> The magnetic susceptibility is almost temperature independent in the C-phase, but it decreases below  $T_c$  when we consider the orbital effect as in §4.1.

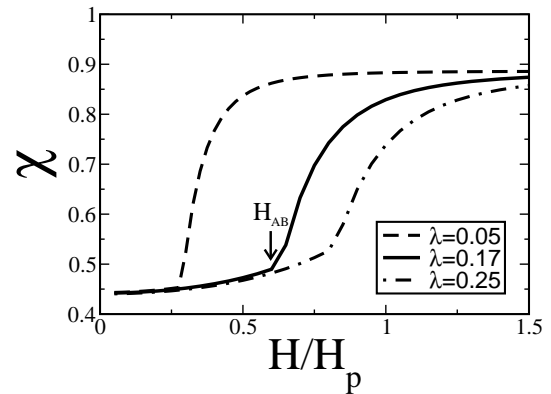


Fig. 5. The magnetic field dependence of magnetic susceptibility at  $T = 0.1T_c^0$ . We show the results for  $\lambda = 0.05$ ,  $\lambda = 0.17$  and  $\lambda = 0.25$ .

Figure 5 shows the magnetic field dependence of magnetic susceptibility. As shown by the arrow, the magnetic susceptibility rapidly increases through the A-B

phase transition. This kink will be visible even if we consider the vortex state as in §4.1. Therefore, the detailed measurement on the magnetic field dependence of NMR Knight shift will be an interesting experiment. If we assume  $\lambda = 0.17$  and  $T_c^0 = 6\text{K}$  as in Fig. 2(b), the A-B transition occurs around  $H = 0.7H_p \sim 6\text{T}$ . This magnetic field is experimentally accessible.

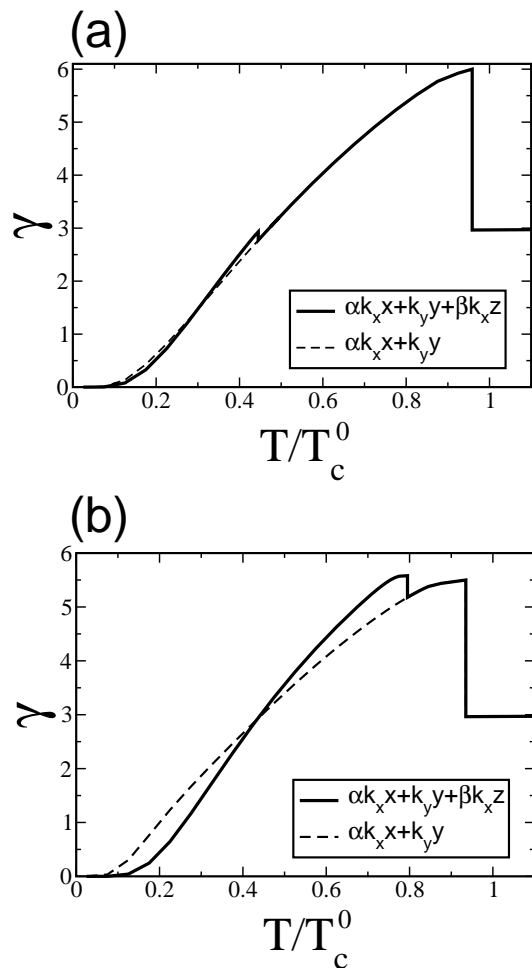


Fig. 6. The temperature dependence of specific heat coefficient  $\gamma = C/T$  (solid line). The dashed line shows the results when we assume the A-phase in whole temperature range. We choose the magnetic field as (a)  $H = 0.7H_p$  and (b)  $H = H_p$ .

Since the A-B transition is the second order phase transition, the specific heat shows a discontinuity. We calculate the specific heat over temperature  $\gamma = C/T$ . The typical behavior is shown in Fig. 6(a) where the discontinuity in  $\gamma$  is not so significant. This is because the entropy is not so different between the A-phase and B-phase. It should be noticed that the A-B phase transition is described by the rotation of  $d$ -vector as shown in Fig. 3 and the amplitude of order parameter changes only slightly. We note that the broadening of the specific heat occurs in the vortex state. Therefore, it may be difficult to observe such a small discontinuity in  $\gamma$  experimentally. Indeed, no evidence has been obtained for the multiple phase transition from the specific heat measurement in  $\text{Na}_x\text{CoO}_2 \cdot y\text{H}_2\text{O}$ .<sup>17-19</sup> However, this is

not incompatible with the existence of multiple phase transition. It is worth noting that the specific heat measurement has not detected the multiple phase transition in  $\text{UPt}_3$  at high fields.<sup>57</sup> If we choose the magnetic field so that the second transition occurs near  $T_c(H)$  as in Fig. 6(b), the discontinuity in  $\gamma$  becomes large. It may be possible to observe the A-B transition in the specific heat measurement by adjusting the magnetic field.

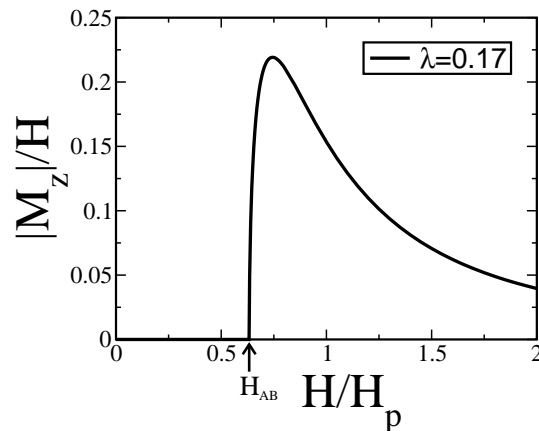


Fig. 7. The magnetization along  $z$ -axis over the magnetic field along  $x$ -axis. The parameters are chosen to be  $T = 0.1T_c^0$  and  $\lambda = 0.17$ .

We find another interesting property of the A-B phase transition, namely the spontaneous rotation of the principal axis of magnetic susceptibility. In the A-phase, the principal axis is the same as the symmetry axis of crystal. On the other hand, the principal axis in the B-phase is misaligned from the crystal axis because the  $d$ -vector having the  $p_x$ -symmetry lies between the  $\hat{x}$  and  $\hat{z}$  direction. This particular property is illuminated by showing the magnetization along the  $z$ -axis,  $M_z$  under the parallel magnetic field. Although the magnetization  $M_z$  is zero in the A-phase and in the normal state,  $M_z$  has a finite value in the B-phase due to the off-diagonal element of susceptibility tensor. We show the magnetic field dependence of  $|M_z|/H_x$  in Fig. 7. The absolute value is shown because the sign of  $M_z$  is different between the 2-fold degenerate states in B-phase (see Table I). It is shown that the magnetization  $|M_z|/H_x$  shows a sharp peak in the B-phase close to the A-B transition. When we increase the magnetic field from the A-B transition line,  $|M_z|/H_x$  first increases owing to the increase of  $\beta$  and then decreases owing to the decrease of  $\alpha$ . Since the appearance of  $|M_z|$  is a particular property of B-phase, the measurement of this quantity will be an interesting experiment. We note that  $|M_z|$  is finite also in the C-phase because of the non-unitarity. However, the value in the C-phase is in the order of  $T_c^0/W$  and therefore much smaller than that in the B-phase.

Thus far, we have assumed  $g_1 - g_5 = 0$ . At the last of this subsection, we discuss the role of the spin-orbit coupling through the finite value of  $g_1 - g_5$ . We fix  $\lambda = 0.17$  as Fig. 2(b) and choose two values of  $g_1 - g_5$  so that  $T_{c2} = 0.825T_c^0$  and  $T_{c2} = 0.905T_c^0$ . Here,  $T_{c2}$  is defined

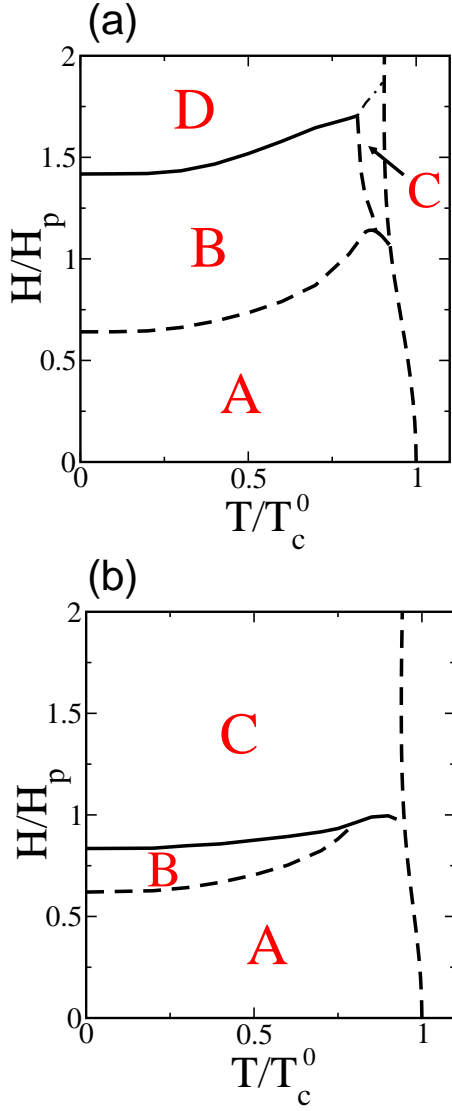


Fig. 8. The phase diagram when the value of  $g_1 - g_5$  is finite. We fix  $\lambda = 0.17$  and choose  $T_{c2} = 0.825T_c^0$  ( $g_1 - g_5 < 0$ ) in (a) and  $T_{c2} = 0.905T_c^0$  ( $g_1 - g_5 > 0$ ) in (b).

as,

$$1 = g_1 \sum_{\mathbf{k}} \frac{|\phi_{1x}(\mathbf{k})|^2}{2E_2(\mathbf{k})} \tanh \frac{E_2(\mathbf{k})}{2T_{c2}}. \quad (8)$$

Since  $T_{c2} = T_c^{(z)} = 0.865T_c^0$  for  $g_1 - g_5 = 0$ ,  $g_1 - g_5 < 0$  in the former case and  $g_1 - g_5 > 0$  in the latter case. Figure 8 shows the phase diagram in each case. In both cases, the phase diagram in the low field region is similar to Fig. 2(b). For instance, the A-B phase transition occurs around  $H = 0.7H_p$ . On the other hand, the pairing state at high magnetic fields is affected by the finite value of  $g_1 - g_5$ . The D-phase is stabilized when  $g_1 - g_5 < 0$  while the C-phase is stabilized when  $g_1 - g_5 > 0$ . These results are understood by noticing that  $g_3$ -term in eq. (3) is ineffective at high magnetic fields since  $\alpha \ll 1$ . Then, the D-phase is favored when the  $g_5$ -term is large while the C-phase is favored when the  $g_1$ -term is large.

As shown in I,<sup>24)</sup> the second order term in  $\lambda$  stabilizes the  $P_{xy+}$ -state furthermore. This means that  $g_1 - g_5 >$

0. Since a large value of  $g_1 - g_5$  has been assumed in Fig. 8(b), the role of  $g_1 - g_5$  may be overestimated. We expect that the C-phase is slightly favored by the finite value of  $g_1 - g_5$  in  $\text{Na}_x\text{CoO}_2 \cdot y\text{H}_2\text{O}$ .

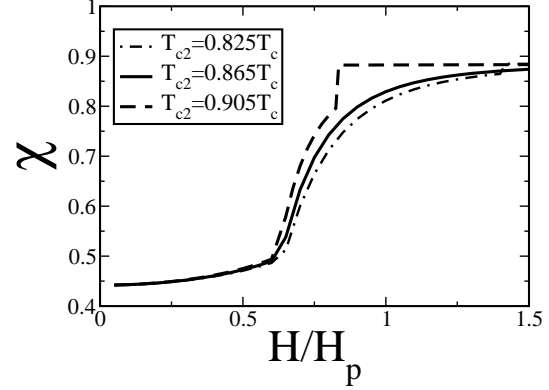


Fig. 9. The magnetic field dependence of magnetic susceptibility at  $T = 0.1T_c^0$  and  $\lambda = 0.17$ . We show the results for  $g_1 - g_5 < 0$ ,  $g_1 - g_5 = 0$  and  $g_1 - g_5 > 0$ , respectively.

Figure 9 shows the field dependence of magnetic susceptibility for  $g_1 - g_5 \neq 0$ . Although the behaviors in the low field region are independent of the value of  $g_1 - g_5$ , the magnetic susceptibility at high fields is affected. The discontinuity appears at the B-D and B-C transition which are the first order phase transition. The magnetic susceptibility in the C- and D-phases does not decrease from the normal state value. We note again that the magnetic susceptibility decreases in the C-phase when we take into account the orbital effect as in §4.1.

### 3.2 *F*-wave state

The phase diagram in the *f*-wave superconducting state is much simpler than the *p*-wave superconducting state. The multiple phase transition is not expected under the magnetic field along the plane even if the  $F_{xy}$ -state is stabilized at  $H = 0$ . Among the 2-fold degeneracy in  $F_{xy}$ -state,  $\hat{d} = \alpha f_2 \hat{x} + f_1 \hat{y}$  is favored by the magnetic field along *x*-axis, as shown in Fig. 10 schematically. Although the magnetic susceptibility slightly decreases owing to the  $\hat{x}$ -component of *d*-vector, the decrease is much less than 1% in our estimation because  $\alpha \ll 1$ .<sup>24)</sup> Then, the level crossing between the  $F_{xy}$ - and  $F_z$ -state due to the Zeeman coupling energy occurs at the extraordinary high magnetic field which will be higher than  $H_{c2}$ .

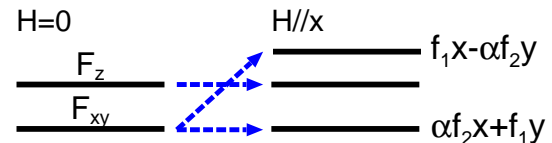


Fig. 10. The schematic figure for the energy level in the *f*-wave superconducting state.

If we apply the magnetic field along *z*-axis, the rota-

tion of  $d$ -vector occurs when the  $F_z$ -state is stabilized at  $H = 0$ . However, it will be difficult to observe this phase transition because the magnetic field is very small owing to the remarkably small splitting of  $T_c$  between  $F_{xy}$ - and  $F_z$ -states, as shown in I.<sup>24)</sup>

From these discussions, it is expected that the single phase would be observed in the  $f$ -wave superconducting state in both directions of magnetic field. We note that almost temperature independent magnetic susceptibility expected in the  $f$ -wave state is incompatible with the results of Co-NMR<sup>9,10,51,52)</sup> and O-NMR.<sup>13)</sup>

### 3.3 $P + F$ -wave state

Finally, we investigate the coexistent  $p + f$ -wave state. We denote this state as E-phase in Table I. In the  $J_H$ - $n_e$  phase diagram in Fig. 1, the coexistent state is stabilized in the region denoted as  $P_{xy+} + F_z$ . Although such a coexistent state with different orbital symmetry is usually realized only accidentally, the  $P_{xy+} + F_z$ -state is stabilized in a relatively large parameter region. This is because the  $p$ -wave and  $f$ -wave superconductivities are nearly degenerate. We have provided a clear explanation on this degeneracy by analyzing the orbital character of six hole pockets.<sup>41)</sup>

In order to investigate the  $p + f$ -wave state in the weak coupling approximation, we consider the  $g_1$ -,  $g_2$ - and  $g_3$ -terms having the  $p$ -wave symmetry and  $g_5$ -term having the  $f_1$ -wave symmetry. Hence,  $g_1 = g_2$  due to the symmetry of triangular lattice, however  $g_4 \neq g_5$  because the  $f_1$ -wave symmetry is not degenerate with the  $f_2$ -wave symmetry which is induced the  $g_4$ -term. Hereafter, we ignore the  $g_4$ -term since the  $T_c$  for the  $f_2$ -wave symmetry is very small.<sup>41)</sup> For simplicity, we assume the orbital wave functions in the  $p_x$ -,  $p_y$ - and  $f_1$ -symmetry as  $\phi_{1x}(\mathbf{k}) = \sqrt{3} \sin \frac{\sqrt{3}}{2} k_x \cos \frac{1}{2} k_y$ ,  $\phi_{1y}(\mathbf{k}) = \sin k_y + \sin \frac{1}{2} k_y \cos \frac{\sqrt{3}}{2} k_x$  and  $\phi_{2y}(\mathbf{k}) = \sin \frac{1}{2} k_y (\cos \frac{1}{2} k_y - \cos \frac{\sqrt{3}}{2} k_x)$ , respectively. These wave functions denote the Cooper pairing between the nearest neighbor sites. The parameters  $g_1 = g_2$ ,  $g_3$  are determined from eqs. (5) and (8) by assuming  $T_{c2} = 0.865T_c^{(xy+)}$  and  $T_c^{(xy+)} = 6\text{K}$ . We choose the critical temperature in the  $f_1$ -wave symmetry, namely  $T_c^{(z)}$  as a parameter and determine  $g_5$  by eq. (6), although  $T_c^{(z)}$  can be determined by the microscopic parameters, such as  $J_H$  and  $n_e$ .

We find three kinds of the  $H$ - $T$  phase diagram which are determined by  $T_c^{(z)}$ . These are classified as (A)  $T_c^{(z)} < T_{c2} < T_c^{(xy+)}$ , (B)  $T_{c2} < T_c^{(z)} < T_c^{(xy+)}$  and (C)  $T_{c2} < T_c^{(xy+)} < T_c^{(z)}$ . Since the case (B) is obtained in the largest parameter range of two-orbital Hubbard model,<sup>24)</sup> we assume the case (B). The phase diagram in this case is shown in Fig. 11.

If we apply the magnetic field along  $x$ -axis, there appears a tetracritical point as in Fig. 11(a). The A-phase is stabilized around  $T = T_c$  at low magnetic fields since  $T_c^{(z)} < T_c^{(xy+)}$ . At high magnetic fields, the F-phase ( $F_z$ -state) is stabilized round  $T = T_c(H)$  since  $T_{c2} < T_c^{(z)}$ . In the low temperature region, the E-phase is stabilized in comparison to the A-phase and F-phase since the superconducting gap is isotropic. The coexistent E-phase

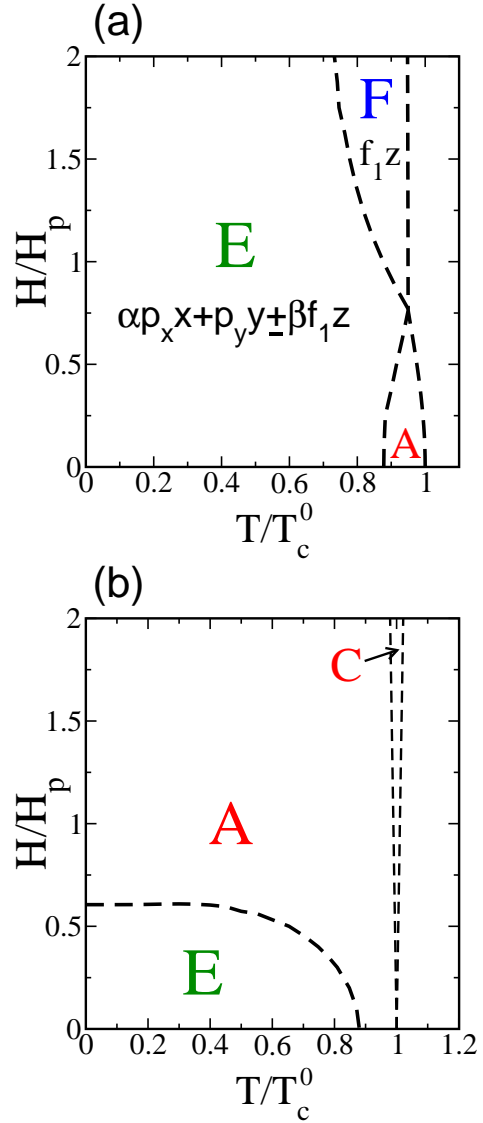


Fig. 11. The  $H$ - $T$  phase diagram in the  $p + f$ -wave superconducting state for (a)  $H \parallel x$  and (b)  $H \parallel z$ . We choose the parameters,  $g_1 = g_2$ ,  $g_3$  and  $g_5$ , so that  $T_{c2} = 0.865T_c^{(xy+)}$  and  $T_c^{(z)} = 0.95T_c^{(xy+)}$ .

appears below the second transition temperature which is lower than  $T_c^{(z)}$ .

We note that Fig. 11(a) is obtained by neglecting the possibility of  $F_{xy}$ -state. The  $F_{xy}$ -state can be stabilized instead of the F-phase when the  $F_{xy}$ -state has higher transition temperature than the  $F_z$ -state. In this case, it is sufficient to substitute the  $F_{xy}$ -state for the  $F_z$ -state in the following discussions. Note that the B-phase and D-phase are not stabilized in the case (B) since  $T_{c2} < T_c^{(z)}$ .

Fig. 11(b) shows the phase diagram under the magnetic field along  $z$ -axis. In this case, we obtain  $\alpha = 1$  in Table I since the symmetry of point group is not reduced. It is shown that the E-phase disappears at high magnetic fields because the magnetic field disfavors the  $d$ -vector along  $z$ -axis. The C-phase is stabilized around  $T = T_c(H)$ . The degeneracy in the C-phase is lifted because the magnetization arising from the non-unitarity couples to the magnetic field. In the present

case,  $\hat{d} = (p_x + ip_y)(\hat{x} - i\hat{y})$  is favored, where only the down spins are superconducting. This is because the DOS at Fermi level is larger for down spins owing to the van-Hove singularity at the Brillouin zone boundary.

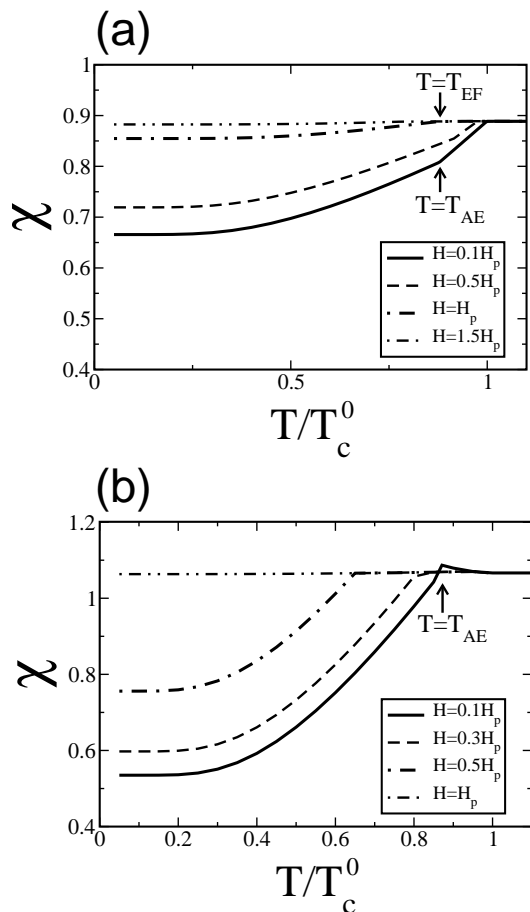


Fig. 12. The temperature dependence of magnetic susceptibility (a) along  $x$ -axis and (b) along  $z$ -axis. We choose the same parameters as in Fig. 11 and the values of magnetic field are shown in the legend. The arrows show the second phase transition.  $T_{AE}$  is the transition temperature from A- to E-phase at  $H = 0.1H_p$  and  $T_{EF}$  is that from E- to F-phase at  $H = H_p$ .

One of the characteristic properties in E-phase is the decrease of magnetic susceptibility *in all directions* of magnetic field. This is because the  $d$ -vector has all components,  $\hat{x}$ ,  $\hat{y}$  and  $\hat{z}$ . We show the temperature dependence of magnetic susceptibility along  $x$ -axis in Fig. 12(a) and that along  $z$ -axis in Fig. 12(b). This feature of E-phase is interesting because the decrease of NMR Knight shift along  $z$ -axis has been reported by Kobayashi *et al.*<sup>10)</sup> This consistency should be contrasted to the  $p$ -wave state (§3.1) and  $f$ -wave state (§3.2) where the magnetic susceptibility along  $z$ -axis does not decrease below  $T_c$ . We note that the magnetic susceptibility does not decrease in the A- and C-phases in Fig. 11(b).

Another important feature of the  $p+f$  coexistent state is the existence of double transition at zero magnetic field. This is in sharp contrast to the phase diagram in the  $p$ -wave state (Fig. 2) which shows no double transition at  $H = 0$ . The second transition from A to E-phase

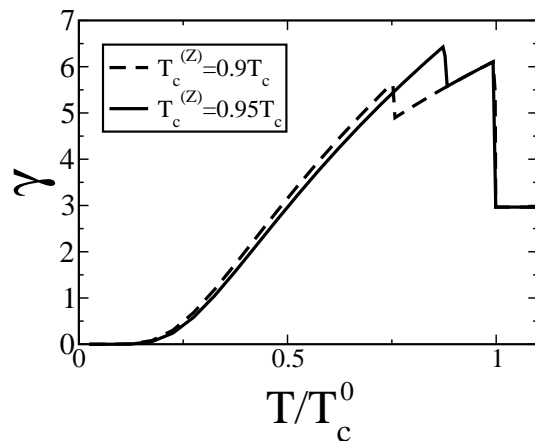


Fig. 13. The temperature dependence of the specific heat coefficient in the  $p+f$ -wave state for two values of  $T_c^{(z)}$ . The solid and dashed lines show the results for  $T_c^{(z)} = 0.95T_c^{(xy+)}$  and  $T_c^{(z)} = 0.9T_c^{(xy+)}$ , respectively. We fix  $T_{c2} = 0.865T_c^{(xy+)}$  and  $H = 0$ .

induces a clear discontinuity of specific heat coefficient  $\gamma$  as shown in Fig. 13. This is because the superconducting gap is much more isotropic in the E-phase than in the A-phase. The  $p$ -wave order parameter is remarkably anisotropic on the  $e_g$ -Fermi surface since both  $p_x$ - and  $p_y$ -wave order parameters vanish around the K-point owing to the periodicity of Brillouin zone. In contrast to that, the  $f_1$ -wave order parameter is almost isotropic on the  $e_g$ -Fermi surface. Therefore, the entropy is significantly reduced by the appearance of  $f$ -wave order parameter. Although the specific heat has been measured at zero magnetic field,<sup>17–19)</sup> no sign of the second phase transition has been reported up to now. We suggest that an experimental search for this second phase transition will be an interesting future issue.

We have calculated the NMR  $1/T_1T$  in the  $p+f$ -wave state, but we can see a very weak anomaly at the second phase transition.<sup>58)</sup> Therefore, it will be difficult to observe this second phase transition by the measurement of NMR  $1/T_1T$ .

#### 4. Roles of Vortex State and $A_{1g}$ -Orbital

In §3, we have ignored two effects which may affect the  $H$ - $T$  phase diagram. One is the orbital effect which induces the vortex state. The other is the role of  $a_{1g}$ -orbital. In this section, we investigate these effects within the qualitative discussion.

##### 4.1 Vortex state

First, we discuss the vortex state. Most of the unconventional superconductors including  $\text{Na}_x\text{CoO}_2 \cdot y\text{H}_2\text{O}$  are classified into type II where the vortex state is stabilized at  $H_{c1} < H < H_{c2}$ . The spatial dependence forming the vortex state is not important for the  $d$ -vector, qualitatively when the orbital part of order parameter has one component. The  $f$ -wave state discussed in §3.2 is the case. However, the  $d$ -vector can be affected by the orbital effect when the orbital part has multi-component as in the  $p$ -wave and  $p+f$ -wave states. In these states, the

$d$ -vector in the vortex state is discussed in the following way.

We discuss the vortex state on the basis of the Ginzburg-Landau theory which provides qualitative and clear understandings. In this theory, the free energy is given by the functional of order parameters as,

$$F = F_0 + F_G, \quad (9)$$

where  $F_0$  is the uniform term and  $F_G$  is the gradient term. Here, we define the order parameters  $d_\alpha^{(\beta)}$  through the  $d$ -vector as  $\hat{d} = \sum_{\alpha\beta} d_\alpha^{(\beta)} \phi_{i\beta}(\mathbf{k}) \hat{\alpha}$  where  $i = 1$  for  $\alpha = x, y$  and  $i = 2$  for  $\alpha = z$ . In this subsection, we analyze the GL functional within the quadratic order and determine the pairing state at  $T = T_c(H)$  and discuss the  $d$ -vector below  $T_c(H)$ .

We first consider the  $p$ -wave superconductivity. Within the quadratic order of uniform term  $F_0$ , there is a 2-fold degeneracy between  $(d_x^{(y)}, d_y^{(x)}) = \Delta_1(\frac{\alpha}{\sqrt{1+\alpha^2}}, -\frac{1}{\sqrt{1+\alpha^2}})$  and  $(d_x^{(x)}, d_y^{(y)}) = \Delta_2(\frac{\alpha}{\sqrt{1+\alpha^2}}, \frac{1}{\sqrt{1+\alpha^2}})$ . These states are obtained from the doubly degenerate  $P_{xy}$ -state in an adiabatic way and nearly degenerate in the A-phase. By taking into account the two component order parameters, namely  $\Delta_1$  and  $\Delta_2$ , the quadratic order term in  $F_0$  is written as  $F_0 = a(T - T_c^{(xy)}(H))(|\Delta_1|^2 + |\Delta_2|^2)$  where  $T_c^{(xy)}(H)$  is the transition temperature obtained in §3.1. Note that the A-phase and C-phase are described by a linear combination of these two component order parameters. We obtain  $(\Delta_1, \Delta_2) \propto (0, 1)$  in the A-phase, and  $(\Delta_1, \Delta_2) \propto (\pm i, 1)$  in the C-phase.

When we consider the magnetic field along  $x$ -axis and ignore the spatial dependence in  $x$ -direction, the gradient term is given as,

$$\begin{aligned} F_G = & K_1^\parallel \{|D_y d_x^{(x)}|^2 + |D_y d_y^{(x)}|^2\} + K_1^\perp |D_y d_z^{(x)}|^2 \\ & + K_2^\parallel \{|D_y d_x^{(y)}|^2 + |D_y d_y^{(y)}|^2\} + K_2^\perp |D_y d_z^{(y)}|^2 \\ & + K_3^\parallel \{|D_z d_x^{(x)}|^2 + |D_z d_y^{(x)}|^2 + |D_z d_x^{(y)}|^2 + |D_z d_y^{(y)}|^2\} \\ & + K_3^\perp \{|D_z d_z^{(x)}|^2 + |D_z d_z^{(y)}|^2\}, \end{aligned} \quad (10)$$

where  $D_j = \partial_j - 2ieA_j$  is the gauge invariant differential operator. The coupling constants are obtained in the clean limit as,  $K_1^\parallel : K_2^\parallel : K_3^\parallel = < |\phi_{1x}(\mathbf{k})|^2 v_y^2 > : < |\phi_{1y}(\mathbf{k})|^2 v_y^2 > : < |\phi_{1x}(\mathbf{k})|^2 v_z^2 >$  and  $K_1^\perp : K_2^\perp : K_3^\perp = < |\phi_{2x}(\mathbf{k})|^2 v_y^2 > : < |\phi_{2y}(\mathbf{k})|^2 v_y^2 > : < |\phi_{2x}(\mathbf{k})|^2 v_z^2 >$  where  $v_\alpha$  is the Fermi velocity along  $\alpha$ -direction and  $<>$  is the average on the Fermi surface. We obtain  $K_i^\parallel \neq K_i^\perp$  in general, but these are nearly the same values because  $\lambda \ll W$ . Therefore, we simply assume  $K_i^\parallel = K_i^\perp = K_i$ . If the cylindrical Fermi surface and purely  $p$ -wave order parameter are assumed, we obtain  $K_2 = 3K_1$ . However, we find that  $K_2 < K_1$  for the Fermi surface relevant for  $\text{Na}_x\text{CoO}_2 \cdot y\text{H}_2\text{O}$ .

It is simply understood that the 2-fold degeneracy between  $\Delta_1$  and  $\Delta_2$  is lifted by taking the gradient term. By taking into account the spatial dependence of order parameters as  $\Delta_1 = \Delta_1(r)$  and  $\Delta_2 = \Delta_2(r)$  and solving the linearized GL equation, we obtain two different  $T_c$

as,

$$T_c^{(xy1)}(H) = T_c^{(xy)}(H) - \frac{2e}{a} \sqrt{\frac{\alpha^2 K_2 + K_1}{1 + \alpha^2}} K_3 H, \quad (11)$$

$$T_c^{(xy2)}(H) = T_c^{(xy)}(H) - \frac{2e}{a} \sqrt{\frac{\alpha^2 K_1 + K_2}{1 + \alpha^2}} K_3 H. \quad (12)$$

The former is the critical temperature for the order parameter  $\Delta_1$ , while the latter is that for  $\Delta_2$ . Since  $K_2 < K_1$  and  $\alpha < 1$ , we obtain

$$T_c^{(xy1)}(H) < T_c^{(xy2)}(H). \quad (13)$$

Thus, the degeneracy between  $\hat{d} = \alpha p_x \hat{x} + p_y \hat{y}$  and  $\hat{d} = \alpha p_y \hat{x} - p_x \hat{y}$  at  $T = T_c(H)$  is lifted by the orbital effect and the former is stabilized. Therefore, the A-phase is always favored rather than the C-phase at  $T = T_c(H)$  in contrast to Fig. 2(b). The C-phase can be stabilized below  $T_c(H)$  through the second order phase transition. This is the most significant role of the orbital effect for the  $d$ -vector.

As for the  $d$ -vector along  $z$ -axis, the degeneracy between  $\hat{d} = p_x \hat{z}$  and  $\hat{d} = p_y \hat{z}$  is lifted by the gradient term in the same way. We obtain the  $T_c$  as,

$$T_c^{(z1)}(H) = T_c^{(z)}(H) - \frac{2e}{a} \sqrt{K_1 K_3} H, \quad (14)$$

$$T_c^{(z2)}(H) = T_c^{(z)}(H) - \frac{2e}{a} \sqrt{K_2 K_3} H, \quad (15)$$

where  $T_c^{(z)}(H)$  is the transition temperature of D-phase without including the orbital effect. We obtain

$$T_c^{(z1)}(H) < T_c^{(z2)}(H), \quad (16)$$

and therefore  $\hat{d} = p_y \hat{z}$  is more favorable than  $\hat{d} = p_x \hat{z}$ . This splitting of transition temperature is due to the difference of coherence length along  $y$ -axis between the  $p_x$ - and  $p_y$ -states. The same mechanism for the splitting of  $T_c$  has been discussed for  $\text{Sr}_2\text{RuO}_4$ .<sup>59)</sup> Then, Agterberg has predicted the double transition at  $H > H_{c1}$ . However, the experimental observation in  $\text{Sr}_2\text{RuO}_4$  is incompatible with the theoretical prediction.<sup>1)</sup> Recently, Udagawa has proposed another idea which resolves this inconsistency.<sup>55)</sup>

Whether  $T_c^{(z2)}(H) < T_c^{(xy2)}(H)$  or not depends on the parameters such as  $K_i$  and  $T_c^{(xy)}(H) - T_c^{(z)}(H)$ . When we assume  $g_1 - g_5 = 0$  as in Fig. 2, we always obtain  $T_c^{(z2)}(H) < T_c^{(xy2)}(H)$ . Then, the A-phase is always stabilized at  $T = T_c(H)$ .

We show the schematic figure of  $H$ - $T$  phase diagram in Fig. 14(a-c). The C-phase appears below  $T_c(H)$  when we assume  $H_{c2} \gg H_p$ . Then, the phase diagram is expected as Fig. 14(a). When  $H_{c2} \gtrsim H_p$ , the C-phase may disappear as in Fig. 14(b). The B-phase is also destabilized by the gradient term at high magnetic fields, however stabilized at low magnetic fields. When  $H_{c2}$  is decreased furthermore, the B-phase disappears as in Fig. 14(c). In this case, another phase  $\hat{d} = p_y \hat{z}$  can be stabilized at high magnetic fields if we assume  $g_1 - g_5 < 0$ . However, this is not expected in our results for the two-orbital Hubbard model.<sup>24)</sup> Unfortunately, there are two different experiment reports for the  $H_{c2}$  in  $\text{Na}_x\text{CoO}_2 \cdot y\text{H}_2\text{O}$ .

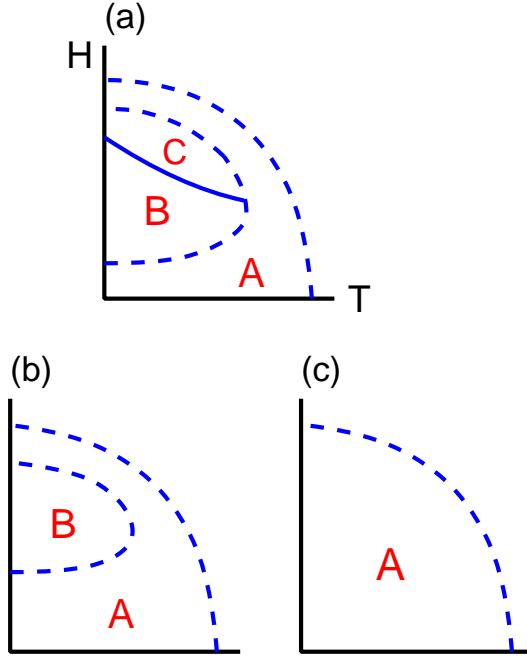


Fig. 14. The schematic figure of  $H$ - $T$  phase diagram in the  $p$ -wave superconducting state when we take into account the vortex state. The magnetic field is applied along  $x$ -axis. The parameter  $H_{c2}/H_p$  is decreased from (a) to (c).

The resistivity measurement has reported  $H_{c2}$  comparable to  $H_p$ ,<sup>20)</sup> while the magnetization measurement has reported  $H_{c2}$  much larger than  $H_p$ .<sup>8)</sup>

The orbital effect in the  $p + f$ -wave state is qualitatively different from the  $p$ -wave state in the sense that  $K_i^{\parallel} \neq K_i^{\perp}$ . In this case, there are two possibilities of the high field phase diagram. When  $\frac{\alpha^2 K_1^{\parallel} + K_2^{\parallel}}{1 + \alpha^2} K_3^{\parallel} > K_2^{\perp} K_3^{\perp}$ , the phase diagram is qualitatively the same as Fig. 11(a). Since the gradient term favors the  $f$ -wave order parameter, the tetracritical point shifts to the lower magnetic field. If we assume  $\frac{\alpha^2 K_1^{\parallel} + K_2^{\parallel}}{1 + \alpha^2} K_3^{\parallel} < K_2^{\perp} K_3^{\perp}$ , the  $f$ -wave order parameter is disfavored by the gradient term. Then, the E-phase disappears in the high field region, and the phase diagram is similar to Fig. 11(b). The microscopic examination of the magnitude relation between  $\frac{\alpha^{\pm} K_1^{\parallel} + K_2^{\parallel}}{1 + \alpha^{\pm}} K_3^{\parallel}$  and  $K_2^{\perp} K_3^{\perp}$  is difficult because it is necessary to estimate  $K_3^{\parallel}$  and  $K_3^{\perp}$  originating from the dispersion relation along  $z$ -axis.

In this paper, we have focused on the phase transition related to the  $d$ -vector and we have not discussed the phase transition in the vortex configuration. Because the vortex lattice structure is sensitive to the pairing state, the latter phase transition may occur in addition. We have simply ignored this possibility because the magnetic and thermodynamic properties are not sensitive to the vortex lattice structure. We think that the more sophisticated and quantitative calculation on the vortex state is one of the fascinating future issues.

#### 4.2 Role of $a_{1g}$ -orbital

We suggest another possibility of phase transition induced by the  $a_{1g}$ -orbital. This phase transition originates

from the 2-fold degeneracy in the  $P_{xy+}$ -state which is related to the  $p$ -wave state (§3.1) and  $p + f$ -wave state (§3.3).

The degeneracy in the  $P_{xy+}$ -state is due to the  $U(1)$  symmetry corresponding to the in-plane rotation of spin.<sup>24)</sup> This symmetry is broken in the three-orbital Hubbard model including the  $a_{1g}$ -orbital because the in-plane component of orbital moment has the matrix element. Therefore, the degeneracy in the two-orbital Hubbard model will be lifted at zero magnetic field. However, it is expected that the lifting of degeneracy is small because the  $a_{1g}$ -orbital is not so important for the superconducting instability.<sup>37,41)</sup> Then, the phase transition can occur in the low magnetic field region.

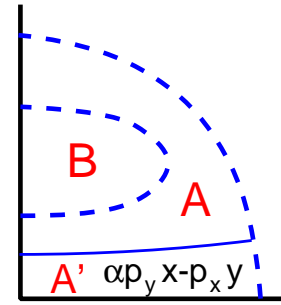


Fig. 15. The schematic figure of  $H$ - $T$  phase diagram when the additional phase transition is induced by the  $a_{1g}$ -orbital. Although we have assumed the  $p$ -wave superconducting state, qualitatively the same phase transition can occur in the  $p + f$ -wave state.

Let us consider the magnetic field along  $x$ -axis. Then, not only the paramagnetic effect (§3) but also the orbital effect (§4.1) favor  $\hat{d} = \alpha p_x \hat{x} + p_y \hat{y}$ , *i.e.* A-phase. Therefore, the level crossing occurs under the magnetic field when the other  $P_{xy+}$ -state, *i.e.*  $\hat{d} = p_y \hat{x} - p_x \hat{y}$ , is stabilized at  $H = 0$ . We show the schematic phase diagram in Fig. 15 where the additional phase transition is assumed.

The experimental identification for this phase transition may be difficult because the magnetic and thermodynamic properties are quite similar between these states. However, we note that this phase transition is associated with the lattice distortion through the electron-phonon coupling. Therefore, this transition may be detected by the measurements such as the magnetostriction, thermal expansion and ultrasonic attenuation and so on. Actually, the multiple phase transition in UPT<sub>3</sub> has been identified by these methods.<sup>60,61)</sup>

## 5. Summary and Discussion

In this paper, we have investigated the multiple superconducting phase transition in the two-orbital Hubbard model representing the  $e'_g$ -orbitals in  $\text{Na}_x\text{CoO}_2 \cdot y\text{H}_2\text{O}$ . We have derived the weak coupling model from the linearized Dyson-Gorkov equation within the second order perturbation theory and solved it within the mean field theory.

In order to determine the pairing state under the magnetic field, we take into account the atomic spin-orbit coupling term as well as the Zeeman coupling term. As a

result of these competing effects, the multiple phase transition occurs in the superconducting state. We have examined the phase diagram in the  $p$ -wave superconductivity,  $f$ -wave superconductivity and their coexistent state, respectively. The obtained phase diagrams are qualitatively different because the role of spin-orbit coupling is quite different between the  $p$ -wave and  $f$ -wave order parameters. The multiple phase transition occurs under the magnetic field along the plane in the  $p$ -wave superconducting state, while that occurs at zero magnetic field in the  $p + f$ -wave state. However, the multiple phase transition does not occur in the  $f$ -wave state. The obtained results are summarized in Table II.

Symmetry	$p$ -wave	$f$ -wave	$p + f$ -wave
Double transition	$H \neq 0$	none	$H = 0$
$K(H \perp z)$	○	×	○
$K(H \parallel z)$	×	×	○

Table II. Summary of the obtained results. The first column shows the pairing symmetry obtained in the multi-orbital Hubbard model. The second column shows the possibility of multiple phase transition. The third and fourth columns show the Knight shift along the plane and along the  $z$ -axis, respectively. The symbol ○ (×) means that the Knight shift decreases (does not decrease) below  $T_c$ .

The characteristics of each pairing state have been illuminated by showing the magnetic susceptibility. When we apply the magnetic field along  $x$ -axis, the magnetic susceptibility decreases in the  $p$ -wave state and in the  $p + f$ -wave state, while that does not decrease in the  $f$ -wave state. The decrease of in-plane Knight shift has been reported by the Co-NMR<sup>9,10,51,52</sup>) and O-NMR<sup>13</sup>) which is consistent with the  $p$ -wave state and  $p + f$ -wave state. When we apply the magnetic field along  $z$ -axis, the magnetic susceptibility decreases in the  $p + f$  coexistent state, while that does not decrease in the  $p$ -wave and  $f$ -wave states. A report of  $c$ -axis Knight shift in the Co-NMR<sup>10</sup>) is consistent with the former.

From these observations, the  $p + f$ -wave state is absolutely consistent with the Knight shift measurements. However, it is still difficult to conclude the pairing state which is consistent with the experimental results in a comprehensive way. A difficulty of the  $p + f$ -wave state is that the second phase transition has not been observed at zero magnetic field. For instance, specific heat<sup>17-19</sup>) measurements have not detected any anomaly. Another difficulty is the power-law behaviors observed in the NMR  $1/T_1T$  and specific heat. Since the superconducting gap is almost isotropic in the  $p + f$ -wave state, the exponential behaviors will be observed in the low temperature region.

Contrary to the  $p + f$ -wave state, the  $p$ -wave superconducting state is consistent with many experimental results except for the  $c$ -axis Knight shift. For instance, the nearly power-law behaviors are expected because the superconducting gap is very anisotropic. This is partly because both  $p_x$ - and  $p_y$ -wave order parameters vanishes around the K-point near the  $e_g$ -Fermi surface, and

furthermore because the nodal quasi-particles exist in the  $a_{1g}$ -Fermi surface. The  $p$ -wave state is also consistent with the  $\mu$ SR measurement<sup>14</sup>) which does not detect any spontaneous time-reversal-symmetry breaking in contrast to  $\text{Sr}_2\text{RuO}_4$ .<sup>49</sup>)

It should be noted that there remain some issues to be resolved when we assume the spin singlet pairing. As for the  $d$ -wave pairing, the  $\mu$ SR measurement is incompatible with the  $d_{xy} + id_{x^2-y^2}$ -wave state which is expected in the triangular lattice.<sup>25-28</sup>) As for the  $i$ -wave pairing,<sup>33</sup>) it seems to be difficult to find a microscopic mechanism which induces such a high angular momentum pairing with  $T_c \sim 5\text{K}$ .

From these discussions, we think that further developments in the theory and experiment are required to identify the pairing symmetry. The experimental search for the multiple phase diagram is particularly interesting because the phase transition related to the  $d$ -vector is a characteristic feature of spin triplet superconductivity. If the multiple phase transition is discovered in the superconducting state, that will be a conclusive evidence for the spin triplet pairing.

In order to suggest future experiments, we have clarified the nature of multiple phase transition. In the  $p$ -wave superconductivity, the A-B transition is promising to be observed. It is shown that the in-plane Knight shift shows a kink at the A-B transition. We find that the magnetization along the  $c$ -axis appears in the B-phase under the in-plane magnetic field. This spontaneous rotation of the principle axis of susceptibility tensor is a characteristic phenomenon in the  $p$ -wave superconducting state.

In order to conclude the  $p + f$ -wave superconductivity, the second phase transition at zero magnetic field should be observed experimentally. The accurate measurement of specific heat around  $T = T_c$  is highly expected because the second transition can be masked by the broadening effect arising from the disorder.

The measurements on the crystal lattice structure are also interesting since the multiple phase transition is associated with the distortion of lattice through the electron-phonon coupling. For instance, the magnetostriction, thermal expansion and ultrasonic attenuation have played an important role in the studies on the heavy fermion superconductors.<sup>60,61</sup>)

In summary, we have examined the possibilities of multiple phase diagram under the parallel magnetic field and suggested some future experiments. We hope that the pairing state in  $\text{Na}_x\text{CoO}_2 \cdot y\text{H}_2\text{O}$  will be resolved by future experiments on the multiple phase transition.

## Acknowledgments

The authors are grateful to Y. Ihara, H. Ikeda, K. Ishida, M. Kato, Y. Kitaoka, Y. Kobayashi, C. Michioka, K. Miyake, Y. Ono, N. E. Phillips, H. Sakurai, M. Sato, M. Udagawa, Y. J. Uemura, K. Yamada, K. Yada and G-q. Zheng for fruitful discussions. Numerical computation in this work was partly carried out at the Yukawa Institute Computer Facility. The present work was partly supported by a Grant-In-Aid for Scientific Research from the Ministry of Education, Science, Sports and Culture, Japan.

- 1) A. P. Mackenzie and Y. Maeno, *Rev. Mod. Phys.* **75** (2003) 657.
- 2) I. J. Lee, S. E. Brown, W. G. Clark, M. J. Strouse, M. J. Naughton, W. Kang and P. M. Chaikin, *Phys. Rev. Lett.* **88** (2002) 017004.
- 3) H. Tou, Y. Kitaoka, K. Asayama, N. Kimura and Y. Onuki: *Phys. Rev. Lett.* **77** (1996) 1374; **80** (1998) 3129.
- 4) K. Ishida, D. Ozaki, T. Kamatsuka, H. Tou, M. Kyogaku, Y. Kitaoka, N. Tateiwa, N. K. Sato, N. Aso, C. Geibel and F. Steglich, *Phys. Rev. Lett.* **89** (2002) 037002.
- 5) S. S. Saxena, P. Agarwal, K. Ahilan, F. M. Grosche, R. K. W. Haselwimmer, M. J. Steiner, E. Pugh, I. R. Walker, S. R. Julian, P. Monthoux, G. G. Lonzarich, A. Huxley, I. Sheikin, D. Braithwaite and J. Flouquet, *Nature* **406** (2000) 587.
- 6) D. Aoki, A. Huxley, E. Ressouche, D. Braithwaite, J. Flouquet, J.-P. Brison, E. Lhotel, C. Paulsen, *Nature* **413** (2001) 613.
- 7) K. Takada, H. Sakurai, E. Takayama-Muromachi, F. Izumi, R. A. Dilanian and T. Sasaki, *Nature* **422** (2003) 53.
- 8) H. Sakurai, K. Takada, S. Yoshii, T. Sasaki, K. Kindo, and E. Takayama-Muromachi, *Phys. Rev. Lett.* **68** (2003) 132507.
- 9) M. Kato, C. Michioka, T. Waki, Y. Itoh, K. Yoshimura, K. Ishida, H. Sakurai, E. Takayama-Muromachi, K. Takada, T. Sasaki, cond-mat/0306036; C. Michioka, M. Kato, K. Yoshimura, K. Takada, H. Sakurai, E. Takayama-Muromachi and T. Sasaki, cond-mat/0403293.
- 10) Y. Kobayashi, M. Yokoi and M. Sato, *J. Phys. Soc. Jpn.* **72** (2003) 2161; 2453; Y. Kobayashi, H. Watanabe, M. Yokoi, T. Moyoshi, Y. Mori, M. Sato, *J. Phys. Soc. Jpn.* **74** (2005) 1800.
- 11) T. Fujimoto, G.-Q. Zheng, Y. Kitaoka, R. L. Meng, J. Cmaidalka and C. W. Chu, *Phys. Rev. Lett.* **92** (2004) 047004.
- 12) K. Ishida, Y. Ihara, Y. Maeno, C. Michioka, M. Kato, K. Yoshimura, K. Takada, T. Sasaki, H. Sakurai and E. Takayama-Muromachi, *J. Phys. Soc. Jpn.* **72** (2003) 3041; Y. Ihara, K. Ishida, C. Michioka, M. Kato, K. Yoshimura, K. Takada, T. Sasaki, H. Sakurai and E. Takayama-Muromachi, *J. Phys. Soc. Jpn.* **73** (2004) 2069.
- 13) Y. Ihara and K. Ishida, K. Yoshimura, K. Takada, T. Sasaki, H. Sakurai and E. Takayama-Muromachi, cond-mat/0506751.
- 14) W. Higemoto, K. Ohishi, A. Koda, S. R. Saha, R. Kadono, K. Ishida, K. Takada, K. Sakurai, E. Takayama-Muromachi and T. Sasaki, *Phys. Rev. B* **70** (2004) 134508.
- 15) Y. J. Uemura, P. L. Russo, A. T. Savici, C. R. Wiebe, G. J. MacDougall, G. M. Luke, M. Mochizuki, Y. Yanase, M. Ogata, M. L. Foo and R. J. Cava, cond-mat/0403031.
- 16) A. Kanigel, A. Keren, L. Patlagan, K. B. Chashka, P. King and A. Amato, *Phys. Rev. Lett.* **92** (2004) 257007.
- 17) H. D. Yang, J.-Y. Lin, C. P. Sun, Y. C. Kang, K. Takada, T. Sasaki, H. Sakurai and E. Takayama-Muromachi, *Phys. Rev. B* **71** (2005) 020504.
- 18) B. Lorenz, J. Cmaidalka, R. L. Meng and C. W. Chu, *Physica C* **402** (2004) 106.
- 19) N. Oeschler, R. A. Fisher, N. E. Phillips, J. E. Gordon, M. L. Foo and R. J. Cava, cond-mat/0409760.
- 20) T. Sasaki, P. Badica, N. Yoneyama, K. Yamada, K. Togano and N. Kobayashi, *J. Phys. Soc. Jpn.* **73** (2004) 1131.
- 21) M. Yokoi, H. Watanabe, Y. Mori, T. Moyoshi, Y. Kobayashi and M. Sato, *J. Phys. Soc. Jpn.* **73** (2004) 1297.
- 22) Y. Ihara, K. Ishida, C. Michioka, M. Kato, K. Yoshimura, K. Takada, T. Sasaki, H. Sakurai and E. Takayama-Muromachi, *J. Phys. Soc. Jpn.* **74** (2005) 867.
- 23) H. Sakurai, K. Takada, T. Sasaki and E. Takayama-Muromachi, preprint.
- 24) Y. Yanase, M. Mochizuki and M. Ogata, cond-mat/0507305.
- 25) G. Baskaran, *Phys. Rev. Lett.* **91** (2003) 097003; D. Sa, M. Sardar and G. Baskaran, *Phys. Rev. B* **70** (2004) 104505.
- 26) B. Kumar and B. S. Shastry, *Phys. Rev. B* **68** (2003) 104508; *Phys. Rev. B* **69** (2004) 059901(E).
- 27) Q.-H. Wang, D.-H. Lee and P. A. Lee, *Phys. Rev. B* **69** (2003) 092504.
- 28) M. Ogata, *J. Phys. Soc. Jpn.* **72** (2003) 1839.
- 29) H. Ikeda, Y. Nisikawa and K. Yamada, *J. Phys. Soc. Jpn.* **73** (2004) 17.
- 30) K. Kuroki, Y. Tanaka and R. Arita, *Phys. Rev. Lett.* **93** (2004) 077001.
- 31) Y. Tanaka, Y. Yanase and M. Ogata, *J. Phys. Soc. Jpn.* **73** (2004) 319.
- 32) O. I. Motrunich and P. A. Lee, *Phys. Rev. B* **69** (2004) 214516; *Phys. Rev. B* **70** (2004) 024514.
- 33) K. Kuroki, Y. Tanaka and R. Arita, *Phys. Rev. B* **71** (2005) 024506.
- 34) K. Yada and Y. Ono, unpublished.
- 35) G. Khaliullin, W. Koshibae and S. Maekawa, *Phys. Rev. Lett.* **93** (2004) 176401.
- 36) W. Koshibae and S. Maekawa, *Phys. Rev. Lett.* **91** (2003) 257003.
- 37) M. Mochizuki, Y. Yanase and M. Ogata, *Phys. Rev. Lett.* **94** (2005) 147005.
- 38) D. J. Singh, *Phys. Rev. B* **61** (2000) 13397; **68** (2003) 020503; M. D. Johannes and D. J. Singh, *Phys. Rev. B* **70** (2004) 014507.
- 39) K.-W. Lee, J. Kuneš and W. E. Pickett, *Phys. Rev. B* **70** (2004) 045104.
- 40) R. Arita, cond-mat/0502256.
- 41) Y. Yanase, M. Mochizuki and M. Ogata, *J. Phys. Soc. Jpn.* **74** (2005) 430.
- 42) D. F. Agterberg, T. M. Rice and M. Sigrist: *Phys. Rev. Lett.* **78** (1997) 3374.
- 43) K. Machida, T. Nishira, T. Ohmi, *J. Phys. Soc. Jpn.* **68** (1999) 3364 and references there in.
- 44) J. A. Sauls, *Adv. Phys.* **43** (1994) 153.
- 45) R. Joynt and L. Taillefer, *Rev. Mod. Phys.* **74** (2002) 235.
- 46) M. Sigrist and K. Ueda, *Rev. Mod. Phys.* **63** (1991) 239.
- 47) Y. Yanase and M. Ogata, *J. Phys. Soc. Jpn.* **72** (2003) 673.
- 48) Y. Yanase, T. Jujo, T. Nomura, H. Ikeda, T. Hotta and K. Yamada, *Phys. Rep.* **387** (2004) 1.
- 49) G. M. Luke, Y. Fudamoto, K. M. Kojima, M. I. Larkin, J. Mermin, B. Nachumi, Y. J. Uemura, Y. Maeno, Z. Q. Mao, Y. Mori, H. Nakamura and M. Sigrist: *Nature* **374** (1998) 558.
- 50) H. Murakawa, K. Ishida, K. Kitagawa, Z. Q. Mao, and Y. Maeno, *Phys. Rev. Lett.* **93** (2004) 167004.
- 51) K. Ishida, private communication.
- 52) G.-Q. Zheng and Y. Kitaoka, private communication.
- 53) C. Michioka and K. Yoshimura, private communication.
- 54) T. Nomura and K. Yamada, *J. Phys. Soc. Jpn.* **71** (2002) 404.
- 55) M. Udagawa, Y. Yanase and M. Ogata, preprint.
- 56) Y. Yanase, M. Mochizuki and M. Ogata, unpublished.
- 57) A. P. Ramirez, N. Stucheli and E. Bucher, *Phys. Rev. Lett.* **74** (1995) 1218.
- 58) Y. Yanase, M. Mochizuki and M. Ogata, unpublished.
- 59) D. F. Agterberg, *Phys. Rev. Lett.* **80** (1998) 5184.
- 60) Y. J. Qian, M.-F. Xu, A. Schenstrom, H.-P. Baum, J. B. Ketterson, D. G. Hinks, M. Levy and B. K. Sarma, *Solid State Commun.* **63** (1987) 599; V. Müller, C. Roth, D. Maurer, E. W. Scheidt, K. Lüders, E. Bücher and H. E. Bömmel, *Phys. Rev. Lett.* **58** (1987) 1224. See also Ref. 45.
- 61) N. H. van Dijk, A. de Visser, J. J. M. Franse, S. Holtmeier, L. Taillefer, J. Flouquet, *Phys. Rev. B* **48** (1993) 1299.